OPTIC DISK AND CUP BOUNDARY DETECTION USING REGIONAL INFORMATION

Gopal Datt Joshi, Jayanthi Sivaswamy

CVIT, IIIT Hyderabad, Hyderabad, India

Kundan Karan, S. R. Krishnadas

Aravind Eye Care System, Madurai, India

ABSTRACT

The shape deformation within the optic disk (OD) is an important indicator for the detection of glaucoma. In this paper, relevant disk parameters are estimated using the OD and cup boundaries. A deformable model guided by regional statistics is used to detect the OD boundary. A cup boundary detection scheme is presented based on the appearance of pallor in *Lab* colour space and the expected cup symmetry. The proposed scheme is tested on 170 images comprising 40 normal and 130 glaucomatous images. The proposed method gives a mean error 0.030 for normal and 0.121 for glaucomatous images in the estimation of cup-to-disk ratio which compares well with reported figures in literature.

***Index Terms*—** Retinal image, Optic Disk, Cup, CDR ratio, Glaucoma

1. INTRODUCTION

Early detection and treatment of retinal diseases are crucial to avoid preventable vision loss. Digital colour fundus (retinal) image (CFI) has emerged as a preferred imaging modality for large scale eye screening programs due to its noninvasive nature. The optic disk (OD) one of the main component of retina (shown in fig 1(a)), is an important indicator for *glaucoma* which is one of the most common causes of blindness. In CFI, OD is a bright region where the optic nerve and blood vessels enter the retina while the cup is a depressed area inside the OD. A quantitative understanding of the shape deformation with-in OD is used for evaluating the progression of glaucoma and hence of interest. Specifically, the Cup-to-disk vertical ratio (CDR) and their area ratio are two important disk parameters of interest, derived using OD and cup boundaries. An automatic measurement of these parameters from CFI could reduce the workload of clinicians and aid objective detection of glaucoma.

The intensity variations within the OD and its vicinity make OD boundary localisation challenging. The cup is primarily defined using 3D depth. Clinicians use high end imaging such as Heidelberg Retina Tomograph (HRT), Optical Coherence Tomography (OCT) to get 3D depth information. Detecting cup boundary from a CFI alone (without 3D depth information) is much more challenging task [1][2]. In many CFIs, estimation of cup boundary is not possible without some experience. Much of prior work on quantification of OD appearance has mainly focused on OD boundary detection whereas handful attempts are made to detect cup boundary. However, detection of both boundaries is a fundamental requirement to estimate disk parameters and therefore to aid detection of glaucoma.

In [3], OD boundary is first manually initialised, and further refined through the free-form GVF-snake. The method presented in [4] uses a point distribution shape model of OD boundary which is derived from training images. The learned shape model is integrated with deformable contour model to obtained OD boundary. *Lowell et al.*[5] uses a elliptical shape based deformable model to extract OD boundary. In [6], an intensity-based template matching is applied to first get a coarse OD boundary and then smoothened by an ellipse fitting step. The above mentioned methods restrict their scope to the OD boundary detection task.

A unified deformable contour approach for OD and cup boundary detection is presented in [1]. This method uses a clustering-based classification of contour points and customised contour evolution step integrated in original snake formulation. Additional 3D depth information is extracted from the CFI stereo pair to get the cup boundary. C/D vertical ratio measurement is reported on only 25 images from a total of 100 images and later compared with the measurements obtained from HRT imaging equipment and from a ophthalmologist. A variational level-set based approach for OD and cup boundary detection is presented in [2]. To best of our knowledge, this is first attempt where assessment of computed C/D vertical ratio is carried out on normal and glaucoma images. A total of 104 images comprising 94 normal and 10 glaucoma patients is used for evaluation. This method uses an elliptical fitting post-processing to handle deformation caused due to blood vessel. In general, the strategy of imposing elliptical shape model [2][6] to handle vessel occlusion fails in accurately localising OD/cup boundary and is also ineffective in capturing local OD boundary variations.

In this paper, we report initial results of a pilot study aimed at robust detection of glaucoma. Towards the aim of computing the CDR, the OD boundary is detected first by using region-based statistics to evolve an active contour [7] instead of using gradient information typically used in existing methods. The use of regional information gives robustness against intensity variations that arise due to vessels.

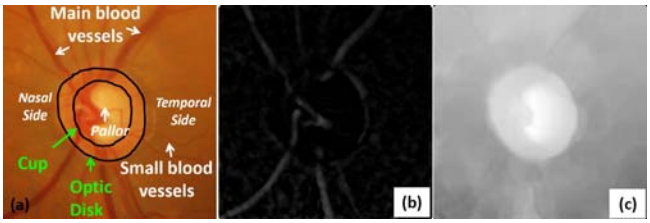

Fig. 1. a) A sample cropped CFI region, b) A max image obtained by morphological closing, c) A vessel-free smooth image.

Moreover, we do not impose any shape constraint on the detected OD and cup boundary. The cup boundary is extracted next using change in colour information near pallor region (brightest region inside OD) and the expected structural symmetry in a cup region. Next, the proposed method is explained in detail followed by details of conducted experiments and obtained results.

2. OPTIC DISK BOUNDARY DETECTION

A coarse localisation of OD region is performed using intensity information from red channel of the CFI as it gives better OD contrast. We linearly transform the image intensity to the range of $0-1$ and extract pixels of value above 0.95. The largest group of connected pixels is selected from the extracted pixels which coincide with brightest region inside OD called pallor. Then, we crop a region around the detected location and use it for further processing. A sample cropped region obtained around the detected OD location is shown in fig. 1(a).

Pre-Processing: From the fig. 1 (a) it can be seen that major blood vessels on the nasal side and small vessel is temporal side present a good amount of OD occlusion. We restore the disk region by significantly reducing the distraction caused by vessels as follows.

We perform bottom-hat transform on red channel I_0 using linear structural elements at different orientations. Bottom-hat transform is the residue between a closing and I_0 defined as: $\rho_s^\theta(I_o) = \varphi_s^\theta(I_o) - I_o$, where φ_s^θ denotes morphological closing operation with a linear structuring element s of orientation θ. The size of structural element is chosen to be larger than the width of major vessels. A max image defined as $I_{max} = \max_\theta \ \rho_s^\theta$ is then obtained, shown in fig. 1(b). A smoothed, vessel-free image is then obtained as $I_p = I_0 + I_{max}$ (see fig. 1(c)). In this image, small artifacts can be seen *only* near the edge of major vessels, however a significant suppression of vessels is achieved.

Region-based Active Contour: Let I_0 be a given image such that $I_0 : \Omega \rightarrow \mathbb{R}$ where Ω be a bounded open subset of $\mathbb{R}^2$, with $\partial\Omega$ the boundary. Let $C(s) : [0,1] \rightarrow \mathbb{R}^2$ be a piecewise parameterized C^1 curve. The active contour model presented in [7] having following form is briefly explained in this section.

$$
\begin{aligned}
F(c^+, c^-, C) \;=\; & \mu \,.\, Length(C) \qquad (1)\\
& + \lambda^+ \int_{inside(C)} |I_0(x,y) - c^+|^2 dxdy \\
& + \lambda^- \int_{outside(C)} |I_0(x,y) - c^-|^2 dxdy
\end{aligned}
$$

where c^+ and c^- are unknown constants representing the average value of I_0 inside and outside the curve, respectively. The parameters $\mu \geq 0$ and $\lambda^+, \lambda^- \geq 0$; are weights for the regularizing and the fitting terms, respectively. Minimizing the fitting error in equ.1, the model looks for the best partition of I_0 taking only two values, namely c^+ and c^-, and with one edge C, the boundary between these two regions, given by $\{I_0 \approx c^+\}$ and $\{I_0 \approx c^-\}$. The object to be detected will be given by one of the regions, and the curve C will be the boundary of the object. The additional length term is a regularizing term and has a scaling role.

For curve evolution, we use level set formulation where the motion is governed by mean curvature. The motion by mean curvature [8] is given by

$$
\begin{cases}
\frac{\partial \phi}{\partial t} = |\nabla \phi| div\left(\frac{\nabla \phi}{|\nabla \phi|}\right) \\
\phi(0,x,y) = \phi_0(x,y), t \in [0,\infty], (x,y) \in \mathbb{R}^2
\end{cases}
$$

where ϕ is the level set function. By this evolution equation, the level curves of ϕ move by a distance mean curvature, in the normal direction.

The original model given in equ.1 can be written in level set formulation. Let the evolving curve be $C = \{(x,y) \in \Omega : \phi(x,y) = 0\}$ assuming that ϕ has opposite signs on each side of C. Using the heaviside function $H(z)$ which takes the value of 1 if $z \geq 0$ or the value of 0 otherwise and $\delta(z) = \frac{d}{dz}H(z)$, energy functional can be re-written as follows:

$$
\begin{aligned}
F(c^+, c^-, \phi) &= \mu \int_\Omega \delta(\phi(x,y)) \, |\nabla \phi(x,y)| \qquad (2)\\
&+ \lambda^+ \int_\Omega |u_0(x,y) - c^+|^2 \, H(\phi(x,y)) dxdy \\
&+ \lambda^- \int_\Omega |u_0(x,y) - c^-|^2 \, (1 - H(\phi(x,y))) dxdy
\end{aligned}
$$

Minimizing the energy $F(c^+, c^-, \phi)$ with respect to ϕ, for fixed c^+ and c^-, using a gradient descent method, yields the associated Euler$-$Lagrange equation for ϕ, governed by the mean curvature and the error terms (see [7] for more details).

On the pre-processed image I_p, we initialise a curve centered at the detected OD location. The curve is evolved based on the average intensity value inside and outside the curve. This model does not use the gradient based stopping criteria thus is robust to gradient variations due to the vessel removal. The curve evolution always converges to the OD boundary irrespective to the shape or size of the initial contour. Fig. 2(a) through (b) shows a sample evolution results where the initial curve was a rectangle.

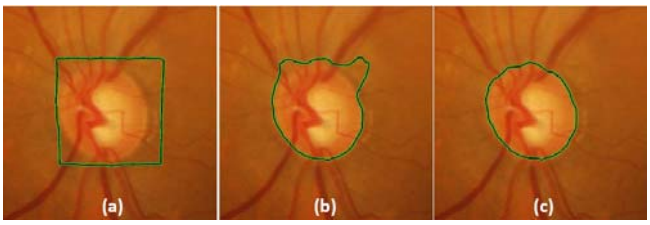

Fig. 2. Active contour at different iterations. a) 20^{th}, b) 200^{th} and c) 380^{th} iterations.

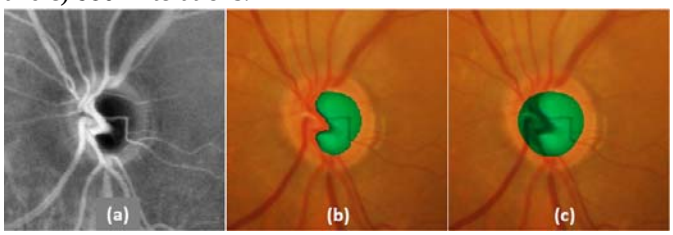

Fig. 3. Cup Segmentation. a) 'a' colour channel in *Lab* colour space, b) Obtained cup pixels after thresholding and c) Recovered cup region.

3. CUP SEGMENTATION

The main visual clues used by clinicians to estimate the cup boundary from CFI are: a) change in colour near pallor boundary and b) bend in small blood vessels. Hence, we make use of color information and structural properties of cup region to get the cup boundary.

Having compared several color spaces, we found the cup region appears most continuous (except major vessel occlusion in nasal side) and well contrasted against the background in the *'a'* plane of the *Lab* color space. For further processing, we take *'a'* colour plane in which cup region appears dark. A morphological opening with a small circular element is carried out to smoothen small blood vessels present in the cup region. Then, we linearly transformed intensity values to the range of [0-1] and extract pixels using a dynamic threshold t to select only pixels which fall inside the OD region. Figure 3(a) shows 'a' colour plane and (b) shows thresholded result overlaid on the original image. The intensity normalisation step and the spatial constraint imposed on the extracted pixels (relevant pixels are always inside OD) make threshold selection trivial. We empirically select a value of $t = 0.07$ which perform consistently well on our dataset.

We use the knowledge about the cup structure to divide the cup into a nasal c_n and temporal c_t regions. The former is generally occluded by the main blood vessels. To recover the same, we impose the expected symmetry of cup region in nasal and temporal side. A vertical axis of symmetry passing through OD center is considered and c_n is obtained via reflection of c_t. The cup boundary is interpolated at high curvature points to get a smoother cup boundary. Consequently, as seen in fig 3(c), the obtained cup region boundary coincides with the bends in small blood vessel. Thus, the detected cup boundary is accurate and corresponds with the visual clues used by the experts.

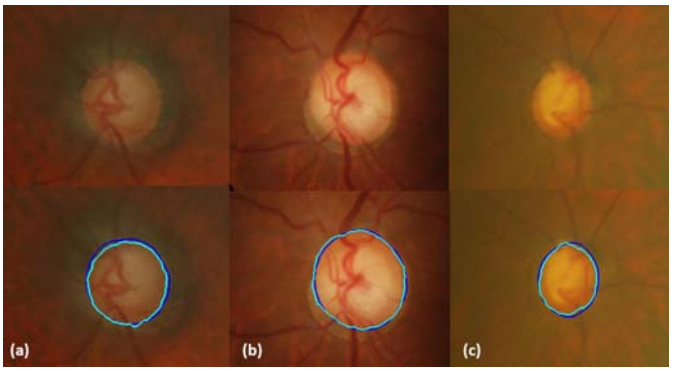

Fig. 4. Obtained optic disk boundary on few challenging cases. Blue: Expert marking; Cyan: Our method

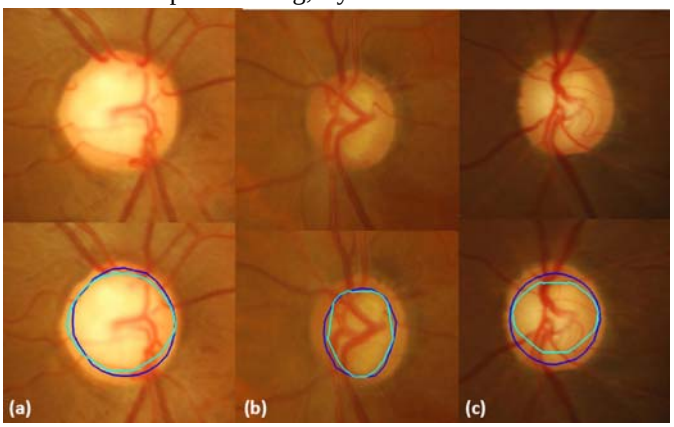

Fig. 5. Obtained cup boundary on few sample images having different OD sizes. Blue: Expert marking; Cyan: Our method

4. EXPERIMENT RESULTS

We evaluate the proposed method's performance on a dataset collected from a local eye hospital as part of an ongoing pilot study. It contains 40 normal and 130 glaucomatous (total of 170) images of size $2896 * 1944$. Images are taken under a fixed protocol with 30-degree field of view centered on the OD. Ground truth (GT) markings for OD and cup boundary are provided by a glaucoma expert.

Evaluation: Figure 4 shows OD boundary detection results on few challenging images overlaid with the boundary marked by an expert. This indicates that the obtained OD boundaries are smooth since region-based active contour is good at handling gradient distortion due to the vessels. Additionally, the method is robust enough to handle paripallary atrophy (concentric bright region around OD; fig 4(a)) and ill-defined OD boundary (fig 4(c)).

Sample results of cup boundary detection are shown in fig. 5 along with GT. The results match well with GT for cases where the expert has used both the pallor and bend in the ves-

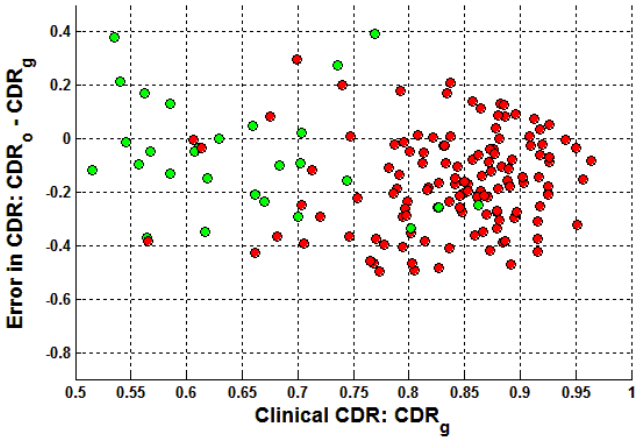

Fig. 6. Error Distribution in CDR estimation against CDR_{gt}. Green: Normal; Red: Glaucomatous Image

sel to mark the cup as in fig 5(a) and not as well when the expert relies only on the latter as in fig 5(c). Under segmentation occurs more in advanced stages of glaucoma marked by a gradual transition between the cup and disc. Here, the pallor is insufficient to define the cup boundary. The density of vessels is maximum in the inferior and superior regions and hence identifying the correct vessel's bend to correct the cup boundary is challenging. A solution is to use 3D depth information.

Since CDR is an important indicator used for glaucoma detection, this metric was chosen to evaluate our results. The CDR is computed with reference to the centroid of the OD region in GT. Let CDR_o and CDR_g be the measures obtained from our method and from GT. Then the error is computed as $E = CDR_o - CDR_g$. From the error distribution plot in fig. 6 it can be seen that the estimation error is lower for normal than for glaucomatous images. The source of this error was found to be consistently in the cup (rather than OD) boundary detection as explained earlier. The average error μ and standard deviation σ of the error for 40 normal and 130 glaucomatous images are shown in Table. 4. The obtained μ/σ are $0.030/0.277$ for normal and $0.121/0.366$ for glaucomatous images. The same figures reported in [2] are $0.082/0.054$ for normal and $0.146/0.077$ for glaucomatous image. Overall, it appears that our method is able to achieve low μ but at higher σ. However, it should be noted that the two datasets differ in a few aspects. The ratio of normal to glaucomatous images in ours and that in [2] are: $1:3.2$, total=170 and $1:9.4$, total=104, respectively.

Given the above figures, we can conclude that our method will give rise to fewer false positives and hence better specificity.

Category	No. of Samples	Mean Error	Standard deviation
Normal	40	0.030	0.277
Glaucoma	130	0.121	0.366
Total	170	0.100	0.348

Table 1. Obtained result's statistics for our method

5. CONCLUSION AND FUTURE DIRECTIONS

In this paper, we present a method to detect OD and cup boundary to get relevant disk parameter for glaucoma detection. In general, the cup deformation is not uniform and the sector where the deformation occurs is also used by experts for glaucoma detection. The ellipse fitting strategy followed by the current methods to obtain the CDR is inadequate for this task. Our method in contrast, can be used to derive this sectorwise information. It needs to be improved to correct for the cup segmentation by including a role for vessel bend.

6. REFERENCES

[1] J. Xu, O. Chutatape, E. Sung, C. Zheng, and P. Chew, "Optic disk feature extraction via modified deformable model technique for glaucoma analysis," *Pattern Recognition*, vol. 40(7), pp. 2063–2076, 2007.

[2] D. Wong, J. Liu, J. Lim, X. Jia, F. Yin, H. Li, and T. Wong, "Level-set based automatic cup-to-disc ratio determination using retinal fundus images in argali," *Proc. EMBC*, pp. 2266–2269, 2008.

[3] F. Mendels, C. Heneghan, and J. P. Thiran, "Identification of the optic disc boundary in retinal images using active contours," *Proc. IMVIP*, pp. 103–115, 1999.

[4] H. Li and O. Chutatape, "A model-based approach for automated feature extraction in fundus images," *IEEE Trans. Biomedical Engineering*, vol. 51(2), pp. 246–254, 2004.

[5] J. Lowell, A. Hunter, D. Steel, A. Basu, R. Ryder, E. Fletcher, and L. Kennedy, "Optic nerve head segmentation," *IEEE Trans. Medical Imaging*, vol. 23(2), pp. 256–264, 2004.

[6] P. Pallawala, W. Hsu, M. Lee, and K. Eong, "Automated optic disc localization and contour detection using ellipse fitting and wavelet transform," *Proc. ECCV*, pp. 139–151, 2004.

[7] T. Chan and L. Vese, "Active contours without edges," *IEEE Trans. Image Processing*, vol. 10(2), pp. 266–277, 2001.

[8] S. Osher and J. Sethin, "Fronts propagating with curvature-dependent speed: Algorithms based on hamilton jacobi formulation," *Journal Comput. Phys.*, vol. 79, pp. 12–49, 1988.